Stochastic tissue environment expands spatial limits of synaptic and astrocytic glutamate actions

Dmitri Rusakov

d.rusakov@ucl.ac.uk

University College London https://orcid.org/0000-0001-9539-9947

Leonid Savtchenko

UCL Institute of Neurology

Thomas Jensen

University College London https://orcid.org/0000-0002-2560-6784

Kaiyu Zheng

University College London https://orcid.org/0000-0002-9002-6292

Article

Keywords:

Posted Date: May 28th, 2025

DOI: https://doi.org/10.21203/rs.3.rs-6066377/v1

Additional Declarations: There is **NO** Competing Interest.

Abstract

The point precision of excitatory transmission relies on high-affinity astrocytic transporters that rapidly buffer glutamate escaping from the synaptic cleft. However, experimental evidence suggests that, in some cases, glutamate can diffuse further away, reaching its receptors at neighbouring synapses. This interpretation challenges the classical paradigm of neural networks operating through strictly one-to-one synaptic connections, yet its biophysical plausibility remains highly debatable. Even less understood is the fate of glutamate reportedly released by astrocytes, as it must bypass the buffering effect of astrocytic transporters located in the immediate vicinity. We theorised that the ongoing debate was partly because existing biophysical models assumed that excitatory synapses are surrounded by transporter-enriched cell elements. In reality, synapses are embedded within a complex environment composed of cellular structures with highly variable shapes and positions, of which only a fraction are astrocytic processes. To address this, we developed and empirically constrained a conceptually novel model of synaptic neuropil *in silico*, where glutamate diffuses and interacts within a stochastically generated tissue environment partially occupied by transporter-expressing astrocytic processes. Our simulations predict that glutamate released from either synapses or astrocytes can potentially activate high-affinity receptors within and beyond a 1-2 μm radius from the release site, thus influencing dozens of nearby synapses. Despite this significant spatial reach, the large discrepancy in the occurrence of glutamatergic vesicles between synapses and astrocytes raises important questions about the physiological relevance of these findings, underscoring the need for further experimental investigation.

MAIN

Glutamatergic synapses have long been considered essential for neural computations, mirroring the one-to-one connectivity central to neural network learning algorithms and electronic memory circuits. To maintain this precision, glutamate escaping the synaptic cleft is rapidly bound by high-affinity transporters, predominantly GLAST/GLT-1 [1-5], which are densely expressed on astrocyte processes permeating the perisynaptic neuropil [6-8]. However, electrophysiological evidence in vitro or in brain slices suggested that glutamate can activate high-affinity receptors up to a few microns from the release site, at least during repetitive or strong stimuli [9-16]. More recent studies using genetically encoded glutamate sensors support this, at least in ex vivo preparations [17-19]. With excitatory synapses separated by just 0.5–0.8 μm [20-23], the observed escape of glutamate suggests the potential for volume-transmitted excitatory signalling. Although the role of volume transmission in neural computation remains largely unexplored, its raising significance is underscored by the evidence of glutamate release by astrocytes [24-27] or at least by certain astrocyte subtypes [28].

The biophysical foundations of these phenomena, essential for the meaningful interpretation of experimental observations, remain highly debated. The membrane surface density of GLT-1 transporters in hippocampal astrocytes is in the region of 10^4 μm^{-2} (refs. [8, 29, 30]). This suggests ~$2{\cdot}10^4$ molecules per 1 μm^3 of neuropil [31] or ~10^5 molecules within ~1 μm of a glutamate release site. This number dwarfs

the estimated 2,000-8,000 glutamate molecules released per synaptic discharge [32-35]. Although anisotropy fluorescence-lifetime imaging (FLIM) measurements suggest that glutamate exhibits relatively high nanoscopic extracellular diffusivity [36], its rapid buffering by GLT-1 likely imposes strong spatial constraints on its actions beyond release sites. The precise amount of glutamate released from astrocytes remains unknown although biochemical, morphological, and physiological evidence suggests it is substantially smaller, or considerably less frequent, than synaptic release [37-41]. Indeed, detailed biophysical models that incorporate the average buffering-and-uptake capacity of GLT-1 distributed across perisynaptic neuropil predicted little glutamate action beyond 0.5-0.7 μm from its release sites [11, 42-46], even with the abundance of obstacle-free escape routes [47]. These estimates have raised potential doubts about the plausibility of interpreting experiments that suggest extended actions of glutamate released by either synapses or astrocytes.

However, astroglial processes occupy only ~10% of neuropil volume [31, 48, 49], with only ~60% of hippocampal synapses having apposing astrocyte processes [50, 51] . This associates GLT-1 expression with relatively small tissue regions, affording potential transporter-free escape routes for glutamate [50, 51] released from either synapses of astrocytes themselves. The prevalence of such escape routes depends on the inherently variable micro-architecture of neuropil, which has been difficult to define or analyse systematically. We therefore hypothesised that the inability of existing biophysical models to account for the substantial spillover of synaptic or astrocytic glutamate arose from the assumption that glutamate transporters are uniformly distributed around synapses.

To mimic the inherent structural variability of neuropil in silico, we developed a stochastic (Monte Carlo) model of synaptic neuropil represented by a random scatter of overlapping spheroids of varied size, with the tortuous extracellular space formed outside [52, 53] (Fig. 1a). The dimensions and volume fractions occupied by spheroid-generated shapes representing neuronal, astroglial, and extracellular space compartments can be tightly constrained by the corresponding experimental values (see below). Critically, each simulation run that tracks the fate of released glutamate molecules generates the local neuropil architecture anew. This approach appears to provide the most realistic representation to date of the inherently variable microenvironment of glutamate release sites in the brain. Our aim was therefore to understand how the diffusion and receptor actions of glutamate released from synapses or astrocytes are constrained by such environment.

RESULTS

Stochastic neuropil model constrained by nanoscopic morphometry

We focused our research on the hippocampal neuropil in area CA1, one of the most common subjects of neuroscience research. In live cortical tissue, ion-sensitive electrode recordings or integrative imaging of extracellular fluorescence have long reported the extracellular space fraction in the region of ~20%, with many interstitial gaps exceeding 100 nm [54-56]. These estimates are consistent with more recent

observations using super-resolution STED imaging or nanoparticle tracking in the extracellular space [57-59]. Both 3D electron microscopy and live super-resolution imaging suggest that the diameter of cellular elements in the synaptic neuropil (axons, dendritic spines, astrocytic processes) is distributed roughly evenly with an average or median in the range 0.3-0.4 μm [51, 57, 60, 61]. When all these parameters were adopted by our spheroid-based model, its 2D-section profiles provided a faithful representation of the extracellular space dimensions and topologies of live hippocampal tissue documented by super-resolution STED shadow-imaging (Fig. 1b).

Adjusting simulation features to experimental design

As noted above, a primary constraint on glutamate diffusion escape is its binding to transporters, receptors, or externally introduced sensors like iGluSnFR [19, 46]. Glutamate binding to such targets is extremely rapid, with rate constants in the range of 10^6-10^7 $M^{-1}s^{-1}$ dwarfing the corresponding unbinding rates. These conditions point to a diffusion-limited process, at least for several milliseconds post-release. Within such limits, the cell-surface binding potency for glutamate is determined by the probability of a binding event once the glutamate molecule occurs in its nanoscopic proximity. In accordance with a Bolzmann distribution, determining this probability can be reduced to the rate parameter Ψ in a Monte Carlo model (Methods), which we have previously validated against experimental receptor-binding data under fast-exchange protocols [32]. In essence, parameter Ψ reflects the density of high-affinity binding sites on cell surfaces.

Thus, once the molecular diffusivity and the features of a stochastically shaped neuropil have been constrained, simulating the spatiotemporal dynamics of free and bound glutamate (Fig. 1c-d) involves one free parameter Ψ. To constrain Ψ using empirical iGluSnFR imaging data, we noted that two-photon excitation (2PE) imaging captures iGluSnFR fluorescence only within an approximately 1 μm thick focal plane. Thus, the optical readout of iGluSnFR fluorescence should correspond to the modelled distribution of iGluSnFR-bound glutamate within a ~1 μm thick tissue slab in the *XY* plane centred at the release site (Fig. 1e).

Constraining the model by empirical data

In hippocampal slices, we traced iGluSnFR-expressing axons from the CA3 pyramidal cell soma projecting towards area CA1 and imaged iGluSnFR signals evoked in their presynaptic boutons by one or several action potentials (Fig. 1f-g; Supplementary Fig. 1), as described previously [19]. Recording images with a millisecond-fast spiral line-scanning method [19, 62] enabled us to obtain spike-evoked iGluSnFR signal profiles with an excellent signal-to-noise ratio and usually a clear hotspot indicating the release site (Fig. 1h; see Methods and further examples in [19]). In each such profile, we calculated the spatial signal decay from the hotspot using 50 nm wide concentric rings (Fig. 1h), arriving at the average dependence for n = 24 synapses (green line and shade in Fig. 1i). We next ran our Monte Carlo model as illustrated (Fig. 1c, d), varying the value of Ψ until the simulated distribution of bound particles in the 1

μm *XY*-plane slab (Fig. 1e) most closely matched the experimental distribution of the iGluSnFR signal (Fig. 1i).

The binding rates of glutamate to GLT-1 transporters and iGluSnFR are on the same scale, and neither the transporters nor the virally expressed iGluSnFR are saturated by individual or low-rate synaptic discharges of glutamate [3, 19, 46, 63]. The optimal Ψ value obtained here (~ 1 ms) thus approximates glutamate buffering potency in the perisynaptic environment, reflecting the density of local GLT-1 and, additionally, the density of glutamate-binding iGluSnFR sites [46] in the immediate axonal membrane. We considered this as a rational starting point for a comparative assessment of glutamate escaping from synapses or astrocytes, under varied distributions of binding sites and amounts of glutamate release.

Concentrating the same number of transporters on astrocytes boost glutamate escape several-fold

In the first round of simulation experiments, we asked how far synaptically released glutamate could exert its actions when astrocytic transporters are distributed evenly across local cell membranes. Given that externally introduced glutamate-iGluSnFR binding in our imaging experiments could have overestimated tissue binding potency [46], we first distributed GLT-1-like binding sites on all spheroid surfaces at a relatively low Ψ = 10 ms. Our simulations then tracked molecules released within the synaptic cleft (Fig. 2a), in 10 separate runs stochastically generating neuropil geometry every time anew. Averaging individual realisations of particle distributions provided the spatiotemporal concentration dynamics of free molecules up to 2 μm from the release site for 10,000 (Fig. 2b) but also for 1000 and 2000 released molecules (Supplementary Fig. 2a). These data were also used to calculate the activity levels of local NMDA receptors by free glutamate (Fig. 2c, Supplementary Fig. 2b). These simulations assumed no Mg^{2+} block at NMDA receptors and that their local concentration was negligible compared to that of GLT-1, so that they could only be activated by free glutamate that escaped GLT-1 binding. The outcome of these tests clearly indicated that having a uniform distribution of GLT-1 in the synaptic neuropil, even at a relatively low density, would restrict glutamate receptor actions to only 0.3-0.5 μm away synapses (Fig. 2c, Supplementary Fig. 2b).

In the next series of tests, we distributed the same amount of GLT-1 as before, but only on the surfaces of astrocyte-associated cell shapes that occupy ~10% of neuropil volume. The latter implied a ten-fold increase in their surface density, or Ψ = 1 ms, to maintain the total of GLT-1, or the average concentration over perisynaptic tissue volume, unchanged. All other simulations settings were as above. The outcome predicted a dramatic boost of glutamate escape compared with the previous case (Fig. 2e, Supplementary Fig. 3a) reflected in a substantially expanded range of NMDA receptor activation (Fig. 2f, Supplementary Fig. 3b).

Glutamate released from either astrocytes or synapses acts over a similar range

While the ability of astrocytes to release glutamate as a molecular signal has long been documented [24-27], the full extent of its actions remains poorly understood. This is primarily due to the difficulty in

distinguishing both the sources and targets of glutamate activity within the neuropil, where synapses and astrocytes exist in nanoscopic proximity.

To explore this scenario, we simulated release of glutamate molecules from the surface of an astrocyte-assigned cellular shape occurring in the centre of the arena (Fig. 3a). For 1000, 2000, and 10000 molecules released, simulations predicted the free glutamate dynamics and NMDA receptor activation profiles that are generally similar to the ones generated by synaptic release (Fig. 3b-c).

Because the neuropil binding capacity, Ψ = 1 ms, estimated in our imaging experiments (Fig. 1i), includes glutamate binding to its sensor, it likely overestimates the total number of binding sites, predominantly GLT-1, in the absence of the sensor. To account for this, and to further explore the parameter range, we simulated glutamate diffusion and receptor interactions following synaptic and astrocytic release of 5000 molecules under conditions where astrocyte-expressed binding sites were halved, by setting Ψ to 2 ms. Once again, simulations demonstrated a comparable range of glutamate escape from synaptic and astrocytic sites (Fig. 4a-b). As expected, the key difference in the glutamate dynamics between the two regimes is that glutamate released from the astrocyte binds in much greater quantities in the release site proximity when released from the astrocyte surface (Fig. 4c).

Overall, the simulation outcomes across varying numbers of released molecules and binding capacities, as illustrated above, offer clear comparative insights into the diffusion and receptor actions of both synaptic and astrocytic glutamate.

DISCUSSION

Bridging the gap between experiments and simulations

The rapid handling and storage of information by brain circuits are thought to rely largely on small glutamatergic synapses and their use-dependent changes in efficacy or strength. One-to-one connections, modifiable by specific activity patterns, appear to provide a sufficient foundation for the full range of tasks performed by artificial neural networks. Consequently, early experimental findings suggesting that, at common central synapses, glutamate can escape the cleft and activate, or at least occupy, receptors on inactive connections [10] raised questions about its functional significance, while also prompting scepticism regarding the reliability of the evidence and its biophysical plausibility. Even when optical glutamate sensors detected traces of glutamate more than a micron away from its release sites, at least in brain slices [18, 19], this seemed to contradict detailed biophysical models that incorporated experimentally validated quantities of high-affinity glutamate transporters by distributing them around active synapses [42, 44, 46].

Reported evidence of evoked glutamate release from astrocytes [24-28, 64] raised even more questions, as glutamate in this context must overcome the buffering capacity of astroglial transporters in its immediate vicinity. One might argue that longer-range actions of astrocytic glutamate could occur in

astrocyte regions lacking transporters, but fluorescently tagged GLT-1 in cell cultures and brain slices reveals a contiguous presence across the astrocytic membrane [65].

Our key hypothesis was that the failure of biophysical models to explain the significant extrasynaptic escape of glutamate observed in experiments stemmed from the assumption that astrocytic glutamate transporters uniformly surround synapses. However, it has long been recognized that astrocytic processes occupy only a portion of the perisynaptic environment, albeit in an unpredictable manner [50, 51]. We therefore developed a novel model of synaptic neuropil, which should capture the stochastic nature and astrocyte specificity of transporter expression near synapses while being tightly constrained by the available experimental data.

Receptor activation by escaped glutamate

Across a range of physiologically plausible parameters for glutamate release and tissue binding capacity, our simulations point to two key findings. Firstly, concentrating glutamate transporters on astroglial processes permits glutamate to escape from synapses over a several-fold greater distance than when transporters are evenly distributed throughout the tissue. Secondly, glutamate released from astrocytes can activate high-affinity receptors more than a micron away from the release site, although this effect strongly depends on the number of molecules released per event.

A key aspect not addressed in the present study is that a portion of glutamate may unbind from its transporters before being taken up into the astrocyte [46]. Previous studies have shown that the relationship between unbinding and uptake rates becomes significant approximately 4 ms after release [66, 67], and our simulations were limited to 8 ms post-release for simplicity. Under conditions similar to the stochastic neuropil modelled here, this secondary wave of unbound glutamate could extend the receptor activation range by 20–30% [67]. While this adjustment does not affect the comparative conclusions of our study, it should be considered when evaluating the broader range of glutamate spillover effects.

The action range of astrocytic glutamate release

A surprising outcome of our simulations is that, under comparable release parameters, glutamate released from astrocytic surfaces can exert effects nearly equivalent to those of glutamate escaping from excitatory synaptic clefts. Given that the nearest-neighbour distance between cortical synapses is approximately 0.5 μm [20], the release of 5000 glutamate molecules, which is the typical amount contained in a single glutamatergic synaptic vesicle [32-35], could activate NMDA receptors up to 1-2 μm away (Fig. 3-4), potentially engaging up to 30 nearby synapses.

Interestingly, NMDA receptor activation exhibits relatively weak dependence on variations in transporter density or the number of molecules released, within reasonable physiological limits (Fig. 3, Supplementary Figs. 2–3). This is because these receptors are primarily activated by the longer-lasting,

low-concentration 'tails' of glutamate transients [20, 46], which, in our case, appear to be shaped by transporter-free escape routes for glutamate.

This raises a critical question: how much glutamate release capacity do astrocytes possess, particularly considering the established evidence for astrocytic vesicular exocytosis [24-28] ? Electron microscopy studies reveal that the number of synaptic vesicles within astrocytes in situ is orders of magnitude lower than that found in neighbouring synapses [37, 39]. However, it is also notable that slow NMDAR-mediated neuronal inward currents (SICs), which have been linked to astrocytic glutamate release in brain slices, are rare compared to typical synaptic discharges [40, 41, 64]. While our simulations indicate that such signalling events are biophysically plausible, their physiological significance remains an open question, warranting further investigation in the intact brain.

METHODS

Animal experimentation

All experiments involving animals were carried out in accordance with the European Commission Directive (86/609/EEC) and the United Kingdom Home Office (Scientific Procedures) Act (1986), under the Home Office Project Licence PP0646543.

Organotypic slice preparation

Organotypic hippocampal slice cultures were prepared from P6–8 Sprague-Dawley rats in accordance with the interface method [68]. We used a Leica VT1200S to section 300 µm thick hippocampal brain slices in ice-cold sterile solution consisting (in mM) of Sucrose 105, NaCl 50, KCl 2.5, NaH_2PO_4 1.25, $MgCl_2$ 7, $CaCl_2$ 0.5, Ascorbic acid 1.3, Sodium pyruvate 3, $NaHCO_3$ 26 and Glucose 10. Following washes in culture media consisting of 50% Minimal Essential Media, 25% Horse Serum, 25% Hanks Balanced Salt solution, 0.5% L-Glutamine, 28 mM Glucose and the antibiotics penicillin (100U/ml) and streptomycin (100 µg/ml), three to four slices were transferred each onto a 0.4 µm pore membrane insert (Millicell-CM, Millipore, UK), kept at 37ºC in 5% CO_2 and fed by medium exchange every 2-3 days for a maximum of 21 days in vitro (DIV). Once ready for experimentation, the slices were transferred to a microscope recording chamber with the recording ACSF solution containing (in mM): NaCl 125, $NaHCO_3$ 26, KCl 2.5, NaH_2PO_4 1.25, $MgSO_4$ 1.3, $CaCl_2$ 2 and glucose 16 (osmolarity 300-305 mOsm), continuously bubbled with 95% O_2/5% CO_2. Recordings were carried out at 33-35C; 10µM NBQX and 50µM AP5 were added to suppress synaptic plasticity effects during prolonged recordings.

iGluSnFR expression

As previously described [19], we expressed the glutamate optical sensor iGluSnFR, including variants SF-iGluSnFR.A184V [69], under a synapsin promoter in CA3 pyramidal cells within organotypic slice cultures using biolistic transfection. In brief, 6.25 mg of 1.6-µm gold microcarriers were coated with 30 µg of the SF-iGluSnFR plasmid. To reduce glial reactivity following transfection, slice cultures at 5 days in vitro

(DIV) were treated overnight with culture media containing 5 μM Ara-C. The following day, the cultures were transfected using a Helios gene gun system (Bio-Rad) at 120 psi. After transfection, the slices were returned to standard culture media and maintained for 5–10 days before conducting experiments.

Tracing and imaging of presynaptic boutons

We used a Femtonics Femto2D-FLIM imaging system, integrated with patch-clamp electrophysiology (Femtonics, Budapest) and linked on the same light path to two femtosecond pulse lasers MaiTai (SpectraPhysics-Newport) with independent shutter and intensity control. Thin-walled borosilicate glass capillaries (GC150-TF, Harvard apparatus) were used to make patch pipettes with an open tip resistance of 2.5-3.5 MΩ. Cell internal solution contained (in mM) 135 potassium methanesulfonate, 10 HEPES, 10 di-Tris-Phosphocreatine, 4 MgCl2, 4 Na2-ATP, 0.4 Na-GTP (pH adjusted to 7.2 using KOH, osmolarity 290–295); Cal-590 (300 μM; AAT Bioquest) was added to enable Ca^{2+} imaging. As detailed previously [19, 62], CA3 pyramidal cells displaying strong iGluSnFR expression under two-photon excitation (at λ_x^{2P}=910 nm) were held in whole cell mode. After 30-45 minutes allowed for Cal-590 equilibration along the cell morphology, the axon was identified and followed, in frame scan mode, to area CA1 where individual presynaptic boutons were identified, first by criteria previously demonstrated [70] and subsequently by their clear ability to release glutamate [19]. To enable millisecond-range imaging of spike-evoked fluorescence dynamics of presynaptic iGluSnFR and Cal-590, a spiral shaped ('Tornado') linescan was placed over the bouton under study, as a built-in scanning option in the Femtonics Femto2D imaging system. The scan rate was set at ~500 Hz, with the power under objective of 3-5 mW. Throughout the trials, the imaged boutons maintained stable morphology, glutamate release and Ca^{2+} signal properties, ruling out any significant photo-toxicity effects. Following a baseline period four APs at 20 Hz were generated using 2 ms positive voltage steps at the cell soma in (V_m holding at -70mV).

Heatmaps of glutamate release

In individual axonal boutons, Tornado scans of green SF-iGluSnFR.A184V and red-shifted Cal-590 signals were collected at ~500 Hz and averaged across individual trials along the corresponding time points in the trial. Scan-average intensity values were used to plot the $\Delta F/F_0$ signal time course, with the basal signal F_0 calculated over the 300 ms pre-pulse interval. To obtain spatial profiles of iGluSnFR.A184V at individual boutons, the recorded Tornado scans were transformed into 2D circular intensity maps by filling in the spaces between spiral turn trajectories with pixels representing a linear transition between the adjacent trajectories (MATLAB function scatteredinterpolant). As the gaps between sequential turns of the spiral trajectories were typically less than 0.2–0.3 μm, which is the light diffraction limit, this procedure introduced no bias or error in the optical signal.

The average $\Delta F/F$ SF-iGluSnFR.A184V heat maps were thus collected during the period between first spike and 15 ms after the fourth spike. The maps represent averaged signals between 5 ms before and 10 ms after each AP-induced peak, thus excluding the troughs of the waveform. Because glutamate binding to iGluSnFR was diffusion-limited whereas unbinding was orders of magnitude slower, this

protocol provided distributions of glutamate binding density with respect to the release site. Because this study was focusing on Euclidean 3D distances, we did not apply a geodesic stereological correction [19]. The glutamate release 'hotspot' location was determined as the area which has top 5% brightness or the peak-intensity pixel location, after 100 nm-radius spatial filtering. Once the hotspot localisation has been determined, the brightness decay was calculated using average intensity values over 50 nm concentric rings centred at the hotspot; areas outside the Tornado circle were ignored.

Model: Generating Probabilistic Synaptic Environment

Monte Carlo simulations were performed within a cubic arena measuring 4 μm per side. To simulate brain neuropil, the space was populated with randomly scattered, overlapping spheroid shapes. This was achieved by generating random 3D coordinates for sphere centroids within the simulation arena, along with random radius values for each sphere. The sphere radii were uniformly distributed between 50 and 300 nm, approximating the sizes of cellular structures observed in electron micrographs and super-resolution images of live brain tissue [51, 57, 60, 61]. This space-generation procedure was repeated independently for each simulation run.

To validate the extracellular tissue volume fraction for each simulation, we (i) randomly distributed ‘test points’ throughout the 3D arena and (ii) calculated the fraction of points falling inside the spheres [52]. Each spheroid was designated as either a neuronal or astroglial element, with probabilities reflecting their respective tissue volume fractions, established empirically. Notably, astrocytic processes were set to occupy approximately 10% of the total volume [31, 48, 49]. The diffusion coefficient for glutamate in the extracellular space was set to D = 0.4 μm²/ms, consistent with in situ measurements of extracellular diffusivity in brain slices obtained through time-resolved fluorescence anisotropy imaging [36]. At the centre of the simulation arena, 1,000 to 10,000 Brownian particles, representing glutamate molecules, were released instantaneously, either from the synaptic cleft (120 nm-wide, 20 nm-high cylindrical disk), or from a 100 nm-wide spot located on the surface of an astrocyte-assigned shape positioned at the arena centre.

Glutamate interaction with neuronal and astroglial surfaces

The interaction between glutamate particles and neuron-assigned spheroids was modelled as an elastic (mirror reflection) collision. In contrast, interactions with astrocyte-assigned spheroids, enriched with high-affinity transporters, were simulated as stochastic binding events occurring with probability *P*. In accordance with statistical physics principles applied to first-order molecular reactions, *P* was defined as a function of time *t* elapsed since the particle’s first collision with the astroglial surface $P = 1 - \exp\left(-t\Psi^{-1}\right)$. Here, Ψ represents the time constant which determines the particle's average dwell time near an astroglial surface for a binding event to occur. Since transporter binding is diffusion-limited due to its high rate, Ψ primarily reflects the density of transporters on the cell surface for a given binding affinity. During the simulations, *P* was computed at every diffusion time step whenever a particle

remained within 5 nm of an astroglial spheroid surface. Immediately after this calculation, a random number was generated to determine, based on the value of *P*, whether the particle would bind or continue to diffuse. Control simulations verified that increasing the cutoff distance beyond 5 nm had no detectable effect on *P* under the simulated conditions. In our previous study, a similar Monte Carlo approach was validated by direct comparison with receptor response data in outside-out patch recordings under a fast-exchange protocol on the sub-millisecond scale of ligand application [32].

NMDA Receptor Activation

Each simulation run typically lasted three milliseconds (system time) post-release, with the trajectories of diffusing Brownian particles tracked at every time step. Following 10 simulation runs, the average numbers of bound and free glutamate molecules were calculated. To determine absolute glutamate concentrations at varying distances from the release site, the numbers of bound and free particles were calculated within concentric rings centred at the arena's midpoint. The extracellular volume within each shell was taken into account to derive the corresponding absolute concentration values. The resulting glutamate concentration dynamics were then used as initial conditions to simulate NMDAR receptor kinetics (assuming no Mg^{2+} block), modelled with five channel states [71]. This was achieved by solving the corresponding system of differential equations, as previously described [20, 71, 72], using MATLAB's built-in 'ode45' solver with a numerical accuracy of balance precision at 10^{-8}, and matching concentration scale at 10^{-20}.

Simulation environment

Monte Carlo simulations were run using either of the two computing environments. The initial testing used a UCL Myriad cluster: processors per node, Intel(R) Xeon(R) Gold 6240 CPU @ 2.60 GHz; cores per node of 36 + 4 A100 GPUs; and RAM per node of 192 GB, tmpfs 1500 G, with a total of 6 nodes. The second environment was cloud computing with Amazon AWS: t4g.medium, with a memory of 4 GB. Parallelisation and optimisation of the algorithms and program codes were implemented by AMC Bridge LLC (Waltham, MA, USA), Unboltsoft (Dnipro, Ukraine), with internet security assistance provided by Cybecurio Ltd. (Berkhamsted, UK).

References

1. Wadiche, J.I., Arriza, J.L., Amara, S.G. & Kavanaugh, M.P. Kinetics of a human glutamate transporter. *Neuron* **14**, 1019-1027 (1995).
2. Zerangue, N. & Kavanaugh, M.P. Flux coupling in a neuronal glutamate transporter. *Nature* **383**, 634-637 (1996).
3. Diamond, J.S. & Jahr, C.E. Transporters buffer synaptically released glutamate on a submillisecond time scale. *J Neurosci* **17**, 4672-4687 (1997).
4. Bergles, D.E. & Jahr, C.E. Glial contribution to glutamate uptake at Schaffer collateral- commissural synapses in the hippocampus. *J. Neurosci.* **18**, 7709-7716 (1998).

5. Auger, C. & Attwell, D. Fast removal of synaptic glutamate by postsynaptic transporters. *Neuron* **28**, 547-558 (2000).
6. Danbolt, N.C.*, et al.* Properties and localization of glutamate transporters. *Prog. Brain Res.* **116**, 23-43 (1998).
7. Rothstein, J.D.*, et al.* Localization of Neuronal and Glial Glutamate Transporters. *Neuron* **13**, 713-725 (1994).
8. Lehre, K.P. & Danbolt, N.C. The number of glutamate transporter subtype molecules at glutamatergic synapses: Chemical and stereological quantification in young adult rat brain. *J. Neurosci.* **18**, 8751-8757 (1998).
9. Asztely, F., Erdemli, G. & Kullmann, D.M. Extrasynaptic glutamate spillover in the hippocampus: Dependence on temperature and the role of active glutamate uptake. *Neuron* **18**, 281-293 (1997).
10. Lozovaya, N.A., Kopanitsa, M.V., Boychuk, Y.A. & Krishtal, O.A. Enhancement of glutamate release uncovers spillover-mediated transmission by N-methyl-D-aspartate receptors in the rat hippocampus. *Neurosci.* **91**, 1321-1330 (1999).
11. Scimemi, A., Fine, A., Kullmann, D.M. & Rusakov, D.A. NR2B-containing receptors mediate cross talk among hippocampal synapses. *J. Neurosci.* **24**, 4767-4777 (2004).
12. Szapiro, G. & Barbour, B. Multiple climbing fibers signal to molecular layer interneurons exclusively via glutamate spillover. *Nature Neurosci.* **10**, 735-742 (2007).
13. Rose, C.R.*, et al.* Astroglial Glutamate Signaling and Uptake in the Hippocampus. *Front Mol Neurosci* **10**, 451 (2017).
14. Chalifoux, J.R. & Carter, A.G. Glutamate Spillover Promotes the Generation of NMDA Spikes. *J. Neurosci.* **31**, 16435-16446 (2011).
15. Hires, S.A., Zhu, Y. & Tsien, R.Y. Optical measurement of synaptic glutamate spillover and reuptake by linker optimized glutamate-sensitive fluorescent reporters. *Proc Natl Acad Sci U S A* **105**, 4411-4416 (2008).
16. Arnth-Jensen, N., Jabaudon, D. & Scanziani, M. Cooperation between independent hippocampal synapses is controlled by glutamate uptake. *Nature Neurosci.* **5**, 325-331 (2002).
17. Henneberger, C.*, et al.* LTP Induction Boosts Glutamate Spillover by Driving Withdrawal of Perisynaptic Astroglia. *Neuron* **108**, 919-936 e911 (2020).
18. Matthews, E.A.*, et al.* Optical Analysis of Glutamate Spread in the Neuropil. *Cereb Cortex* **32**, 3669–3689 (2022).
19. Jensen, T.P.*, et al.* Multiplex imaging relates quantal glutamate release to presynaptic Ca2+ homeostasis at multiple synapses in situ. *Nature Communications* **10**, 1414 (2019).
20. Rusakov, D.A. & Kullmann, D.M. Extrasynaptic glutamate diffusion in the hippocampus: ultrastructural constraints, uptake, and receptor activation. *J. Neurosci.* **18**, 3158-3170 (1998).
21. DeFelipe, J., Marco, P., Busturia, I. & Merchan-Perez, A. Estimation of the number of synapses in the cerebral cortex: methodological considerations. *Cereb Cortex* **9**, 722-732 (1999).

22. Santuy, A.*, et al.* Estimation of the number of synapses in the hippocampus and brain-wide by volume electron microscopy and genetic labeling. *Sci Rep* **10**, 14014 (2020).
23. Montero-Crespo, M.*, et al.* Three-dimensional synaptic organization of the human hippocampal CA1 field. *Elife* **9** (2020).
24. Bezzi, P.*, et al.* Prostaglandins stimulate calcium-dependent glutamate release in astrocytes. *Nature* **391**, 281-285 (1998).
25. Araque, A., Li, N., Doyle, R.T. & Haydon, P.G. SNARE protein-dependent glutamate release from astrocytes. *J Neurosci* **20**, 666-673 (2000).
26. Parpura, V. & Haydon, P.G. Physiological astrocytic calcium levels stimulate glutamate release to modulate adjacent neurons. *Proc Natl Acad Sci U S A* **97**, 8629-8634 (2000).
27. Takano, T.*, et al.* Receptor-mediated glutamate release from volume sensitive channels in astrocytes. *Proc Natl Acad Sci U S A* **102**, 16466-16471 (2005).
28. de Ceglia, R.*, et al.* Specialized astrocytes mediate glutamatergic gliotransmission in the CNS. *Nature* **622**, 120-129 (2023).
29. Furness, D.N.*, et al.* A Quantitative Assessment of Glutamate Uptake into Hippocampal Synaptic Terminals and Astrocytes: New Insights into a Neuronal Role for Excitatory Amino Acid Transporter 2 (Eaat2). *Neurosci.* **157**, 80-94 (2008).
30. Radulescu, A.R.*, et al.* Estimating the glutamate transporter surface density in distinct sub-cellular compartments of mouse hippocampal astrocytes. *PLoS Comput Biol* **18**, e1009845 (2022).
31. Lehre, K.P. & Rusakov, D.A. Asymmetry of glia near central synapses favors presynaptically directed glutamate escape. *Biophys J* **83**, 125-134 (2002).
32. Savtchenko, L.P., Sylantyev, S. & Rusakov, D.A. Central synapses release a resource-efficient amount of glutamate. *Nature Neurosci.* **16**, 10-U163 (2013).
33. Wang, Y.*, et al.* Counting the Number of Glutamate Molecules in Single Synaptic Vesicles. *J Am Chem Soc* **141**, 17507-17511 (2019).
34. Durst, C.D.*, et al.* Vesicular release probability sets the strength of individual Schaffer collateral synapses. *Nat Commun* **13**, 6126 (2022).
35. Diamond, J.S. & Jahr, C.E. Synaptically released glutamate does not overwhelm transporters on hippocampal astrocytes during high-frequency stimulation. *J Neurophysiol* **83**, 2835-2843 (2000).
36. Zheng, K.Y.*, et al.* Nanoscale diffusion in the synaptic cleft and beyond measured with time-resolved fluorescence anisotropy imaging. *Scientific Reports* **7**, 42022 (2017).
37. Bezzi, P.*, et al.* Astrocytes contain a vesicular compartment that is competent for regulated exocytosis of glutamate. *Nat Neurosci* **7**, 613-620 (2004).
38. Li, D.*, et al.* Lack of evidence for vesicular glutamate transporter expression in mouse astrocytes. *J Neurosci* **33**, 4434-4455 (2013).
39. Bergersen, L.H.*, et al.* Immunogold detection of L-glutamate and D-serine in small synaptic-like microvesicles in adult hippocampal astrocytes. *Cereb Cortex* **22**, 1690-1697 (2012).

40. D'Ascenzo, M.*, et al.* mGluR5 stimulates gliotransmission in the nucleus accumbens. *Proc Natl Acad Sci U S A* **104**, 1995-2000 (2007).
41. Shigetomi, E., Bowser, D.N., Sofroniew, M.V. & Khakh, B.S. Two forms of astrocyte calcium excitability have distinct effects on NMDA receptor-mediated slow inward currents in pyramidal neurons. *J. Neurosci.* **28**, 6659-6663 (2008).
42. Barbour, B. An evaluation of synapse independence. *J. Neurosci.* **21**, 7969-7984 (2001).
43. Rusakov, D.A. The role of perisynaptic glial sheaths in glutamate spillover and extracellular Ca^{2+} depletion. *Biophys J* **81**, 1947-1959 (2001).
44. Franks, K.M., Bartol, T.M. & Sejnowski, T.J. An MCell model of calcium dynamics and frequency-dependence of calmodulin activation in dendritic spines. *Neurocomputing* **38**, 9 (2001).
45. Zheng, K., Scimemi, A. & Rusakov, D.A. Receptor actions of synaptically released glutamate: the role of transporters on the scale from nanometers to microns. *Biophysical Journal* **95**, 4584-4596 (2008).
46. Armbruster, M., Dulla, C.G. & Diamond, J.S. Effects of fluorescent glutamate indicators on neurotransmitter diffusion and uptake. *Elife* **9** (2020).
47. Savtchenko, L.P., Zheng, K.Y. & Rusakov, D.A. Buffering by Transporters Can Spare Geometric Hindrance in Controlling Glutamate Escape. *Frontiers in Cellular Neuroscience* **15** (2021).
48. Savtchenko, L.P.*, et al.* Disentangling astroglial physiology with a realistic cell model in silico. *Nature Communications* **9**, 3554 (2018).
49. Minge, D.*, et al.* Heterogeneity and Development of Fine Astrocyte Morphology Captured by Diffraction-Limited Microscopy. *Front Cell Neurosci* **15**, 669280 (2021).
50. Ventura, R. & Harris, K.M. Three-dimensional relationships between hippocampal synapses and astrocytes. *J. Neurosci.* **19**, 6897-6906 (1999).
51. Witcher, M.R.*, et al.* Three-dimensional relationships between perisynaptic astroglia and human hippocampal synapses. *Glia* **58**, 572-587 (2010).
52. Savtchenko, L.P., Zheng, K. & Rusakov, D.A. Conductance of porous media depends on external electric fields. *Biophys J* **120**, 1431-1442 (2021).
53. Savtchenko, L.P. & Rusakov, D.A. Increased Extrasynaptic Glutamate Escape in Stochastically Shaped Probabilistic Synaptic Environment. *Biomedicines* **10**, 2406 (2022).
54. Rice, M.E. & Nicholson, C. Diffusion Characteristics and Extracellular Volume Fraction during Normoxia and Hypoxia in Slices of Rat Neostriatum. *J. Neurophysiol.* **65**, 264-272 (1991).
55. Thorne, R.G. & Nicholson, C. In vivo diffusion analysis with quantum dots and dextrans predicts the width of brain extracellular space. *Proc. Natl. Acad. Sci. USA* **103**, 5567-5572 (2006).
56. Sykova, E. & Nicholson, C. Diffusion in brain extracellular space. *Physiol. Rev.* **88**, 1277-1340 (2008).
57. Tonnesen, J., Inavalli, V. & Nagerl, U.V. Super-Resolution Imaging of the Extracellular Space in Living Brain Tissue. *Cell* **172**, 1108-1121 e1115 (2018).

58. Grassi, D.*, et al.* Nanoscale and functional heterogeneity of the hippocampal extracellular space. *Cell Rep* **42**, 112478 (2023).
59. Paviolo, C.*, et al.* Nanoscale exploration of the extracellular space in the live brain by combining single carbon nanotube tracking and super-resolution imaging analysis. *Methods* **174**, 91-99 (2020).
60. Shepherd, G.M.G. & Harris, K.M. Three-dimensional structure and composition of CA3 -> CA1 axons in rat hippocampal slices: Implications for presynaptic connectivity and compartmentalization. *J. Neurosci.* **18**, 8300-8310 (1998).
61. Tonnesen, J., Katona, G., Rozsa, B. & Nagerl, U.V. Spine neck plasticity regulates compartmentalization of synapses. *Nat Neurosci* **17**, 678-685 (2014).
62. Jensen, T.P., Zheng, K., Tyurikova, O., Reynolds, J.P. & Rusakov, D.A. Monitoring single-synapse glutamate release and presynaptic calcium concentration in organised brain tissue. *Cell Calcium* **64**, 102-108 (2017).
63. Armbruster, M., Hanson, E. & Dulla, C.G. Glutamate Clearance Is Locally Modulated by Presynaptic Neuronal Activity in the Cerebral Cortex. *J. Neurosci.* **36**, 10404-10415 (2016).
64. Serra, I.*, et al.* Astrocyte ensembles manipulated with AstroLight tune cue-motivated behavior. *Nat Neurosci* (2025).
65. Michaluk, P., Heller, J.P. & Rusakov, D.A. Rapid recycling of glutamate transporters on the astroglial surface. *Elife* **10**, 64714 (2021).
66. Bergles, D.E., Tzingounis, A.V. & Jahr, C.E. Comparison of coupled and uncoupled currents during glutamate uptake by GLT-1 transporters. *J Neurosci* **22**, 10153-10162 (2002).
67. Savtchenko, L.P. & Rusakov, D.A. Rapid glutamate unbinding from its transporters can boost activation of distant NMDA receptors. *Cells*, (in press) (2023).
68. Stoppini, L., Buchs, P.A. & Muller, D. A simple method for organotypic cultures of nervous tissue. *J. Neurosci. Meth.* **37**, 173-182 (1991).
69. Marvin, J.S.*, et al.* Stability, affinity, and chromatic variants of the glutamate sensor iGluSnFR. *Nature Methods* **15**, 936-939 (2018).
70. Rusakov, D.A. & Fine, A. Extracellular Ca^{2+} depletion contributes to fast activity-dependent modulation of synaptic transmission in the brain. *Neuron* **37**, 287-297 (2003).
71. Clements, J.D., Lester, R.A., Tong, G., Jahr, C.E. & Westbrook, G.L. The time course of glutamate in the synaptic cleft. *Science* **258**, 1498-1501 (1992).
72. Zheng, K. & Rusakov, D.A. Efficient integration of synaptic events by NMDA receptors in three-dimensional neuropil. *Biophysical Journal* **108**, 2457-2464 (2015).

Figures

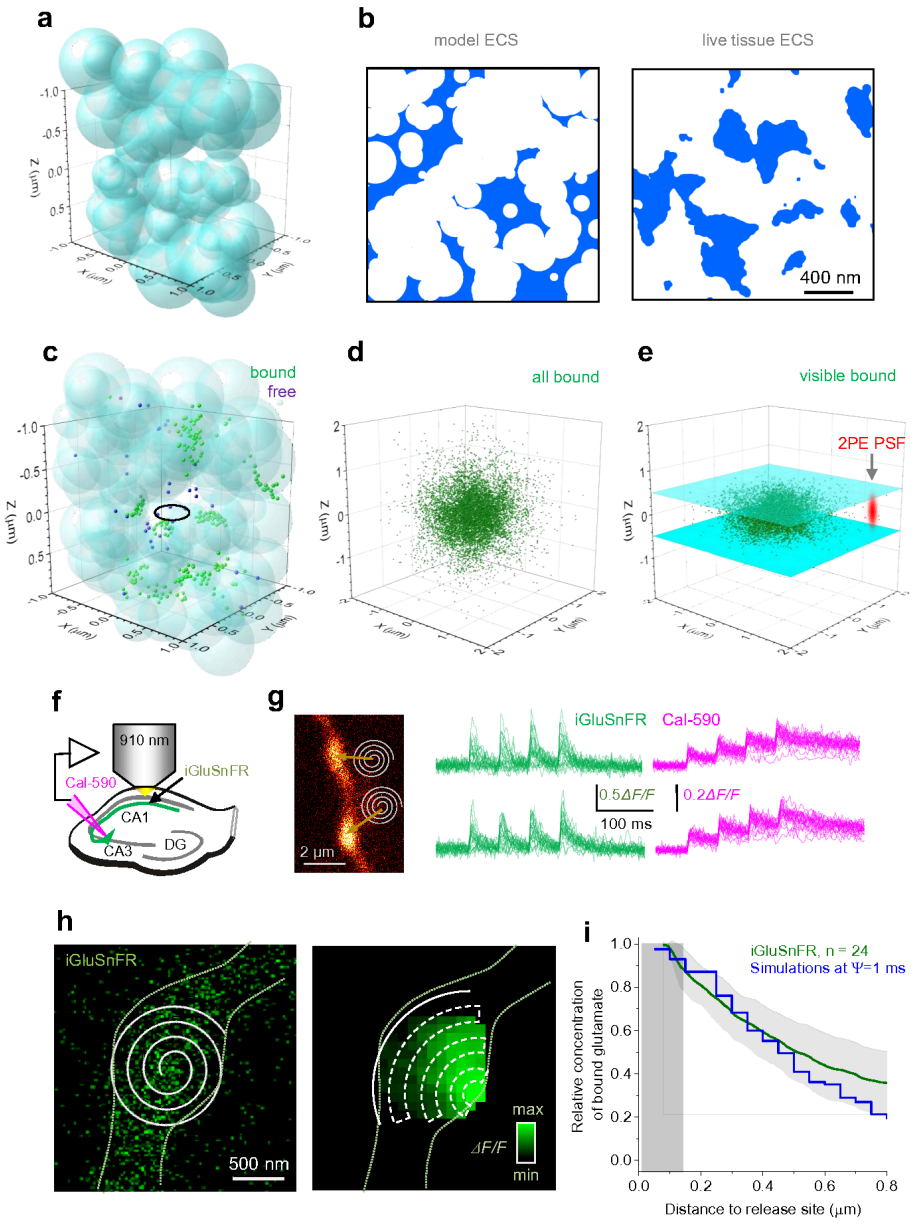

Figure 1

Simulating glutamate release, diffusion and binding in stochastic neuropil constrained by experimental data.

(a) Illustration of the neuropil model (0.5 µm thick slab example) generated stochastically as a random scatter of overlapping spheres, with the dimensions and volume fractions constrained by empirical data.

(b) Example of a random 2D section through the modelled neuropil, as in **a** (*left*), and within the two-photon excitation focal plane imaged using shadow-imaging STED microscopy in hippocampal slices (*right*, adapted from [57]); blue, extracellular space.

(c) A snapshot example of simulation outcome depicting the distribution of bound (green) and free (blue) particles (glutamate molecules) 3.7 ms after instantaneous release in the central synaptic cleft (see text); a 0.5 μm thick 2 μm wide fragment of the 4 x 4 μm^2 simulation arena is shown; 10000 particles released; see Methods for further detail.

(d) Simulated volume distribution of bound particles (glutamate molecules) as in **c**, but across the entire simulation arena; neuropil cell shapes are omitted for clarity.

(e) Example as in **d**, but with the particle visualisation limited by the 1 μm thick slab centred at the release site, to mimic the typical point spread function (PSF) depth of a two-photon excitation (2PE) microscope, which defines the focal plane.

(f) Experimental design, as detailed in Methods and [19], with CA3 pyramidal cells held whole cell in organotypic hippocampal slices.

(g) Image panel: Example of presynaptic boutons of CA3 pyramidal cell axons projected towards area CA1 (iGluSnFR channel), with the positioning of Tornado scans depicted; see Supplementary Fig. 1 and [19] for complete examples.

(h) Example of a presynaptic bouton of the CA3 pyramidal cell axon with a Tornado scan place over it (*left*) and the accumulated average iGluSnFR signal heatmap, with an illustration of concentric rings (not to scale) for intensity measurements (r*ight*); see Methods for details.

(i) Matching the simulated distribution of bound glutamate molecules in the stochastic neuropil model (blue line) with the experimental distribution of iGluSnFR signal intensity (green line; shade mean ± SEM, n = 24), with respect to the release site.

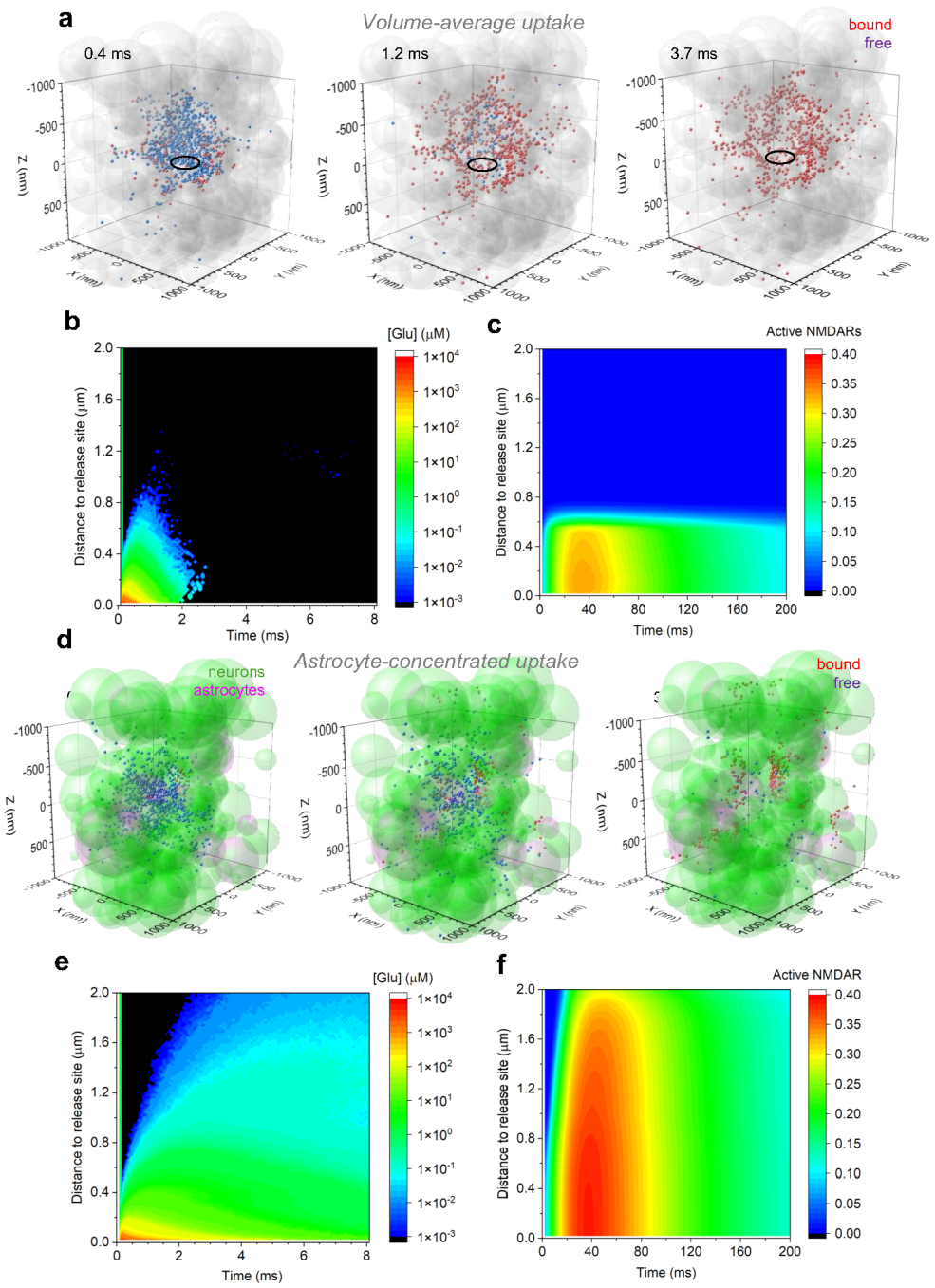

Figure 2

Expressing transporters on astrocyte protrusions, rather across the tissue, increases glutamate escape several-fold.

(a) Snapshot examples illustrating simulated distributions of bound (red balls) and free (blue balls) glutamate molecules at various time after an instantaneous release of 10000 in the centre of the

synaptic cleft (oval); neuropil parameters as in Fig. 1a (see Methods); glutamate transporters are distributed across all cell surfaces at a density which corresponds to Ψ = 10 ms; 2 x 2 μm^2 fragment of the 4 x 4 μm^2 simulation arena is shown.

(b) The spatiotemporal dynamics of the free glutamate concentration in simulation experiments illustrated in **a**.

(c) The spatiotemporal dynamics of NMDA receptor activation, assuming no Mg^{2+} block, computed based on the free glutamate dynamics as shown in **b**; see Methods for further detail.

(d) Snapshot examples illustrating simulated distributions of bound (red balls) and free (blue balls) glutamate molecules at various time after an instantaneous release of 10000 in the centre of the synaptic cleft (oval). Simulated neuropil includes neuronal (green) and astroglial (pink) cell elements, as indicated. Glutamate transporters are distributed on astroglial element surfaces only (volume fraction ~10%), at a density which corresponds to Ψ = 1 ms; other parameters as in **a**.

(e) The spatiotemporal dynamics of the free glutamate concentration in simulation experiments illustrated in **d**.

(f) The spatiotemporal dynamics of NMDA receptor activation, assuming no Mg^{2+} block, computed based on the free glutamate dynamics as shown in **e**; see Methods for further detail.

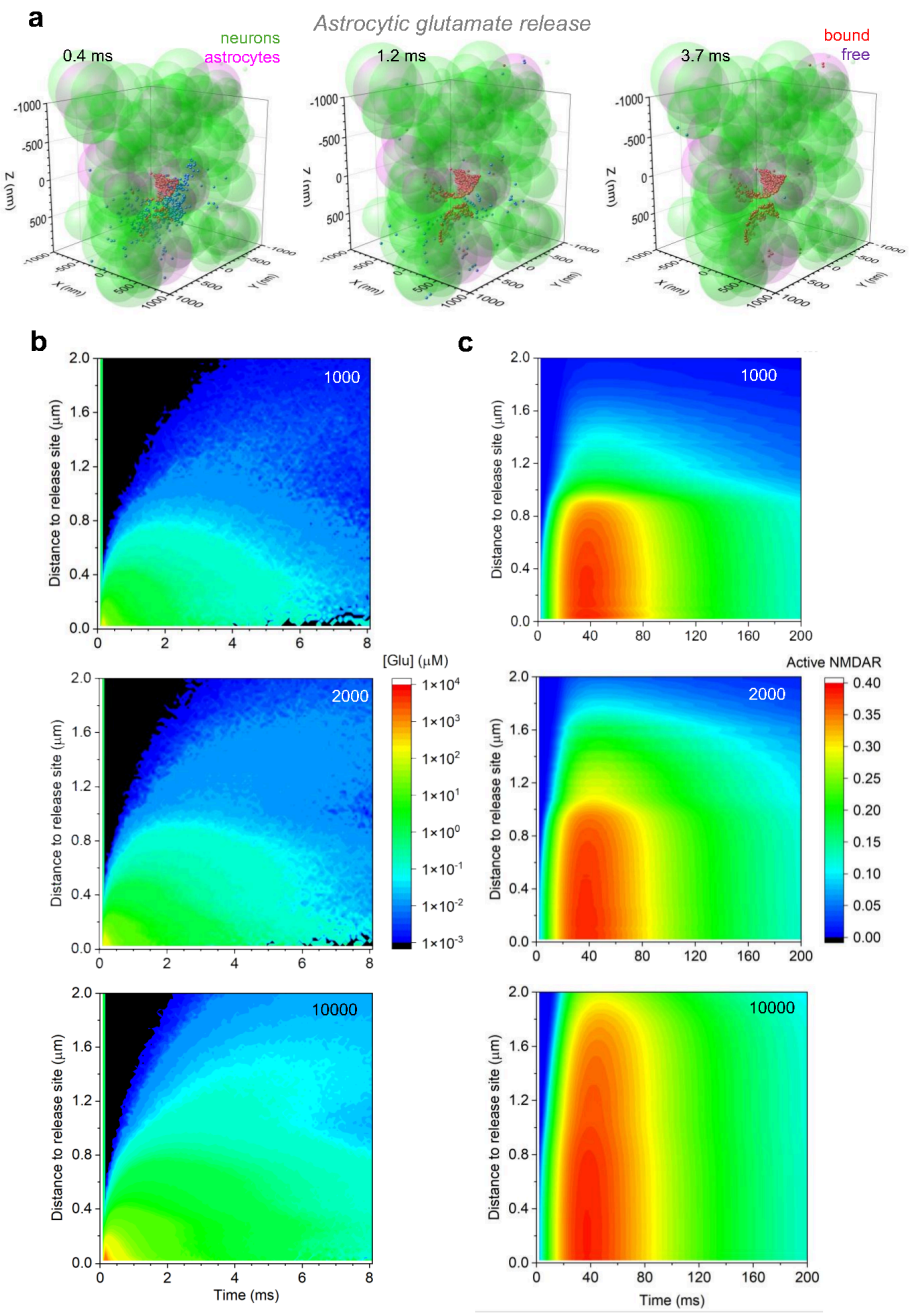

Figure 3

Escape of glutamate released from astrocytes.

(a) Snapshot examples illustrating simulated distributions of bound (red balls) and free (blue balls) glutamate molecules in the neuropil consisting of neuronal (green) and astroglial (pink) cell elements, at various times after an instantaneous release of 10000 from the surface (5 x 5 nm^2 area) of an astroglial

element in the centre. Glutamate transporters are distributed on the astroglial element surfaces only (volume fraction ~10%), at a density which corresponds to Ψ = 1 ms; 2 x 2 μm^2 fragment of the 4 x 4 μm^2 simulation arena is shown.

(b) The spatiotemporal dynamics of the free glutamate concentration in simulation experiments illustrated in **a**, in conditions when 1000, 2000, or 10000 glutamate molecules were released, as indicated.

(c) The spatiotemporal dynamics of NMDA receptor activation, assuming no Mg^{2+} block, computed based on the free glutamate dynamics as shown in b, for the corresponding numbers of released glutamate molecules, as indicated; see Methods for further detail.

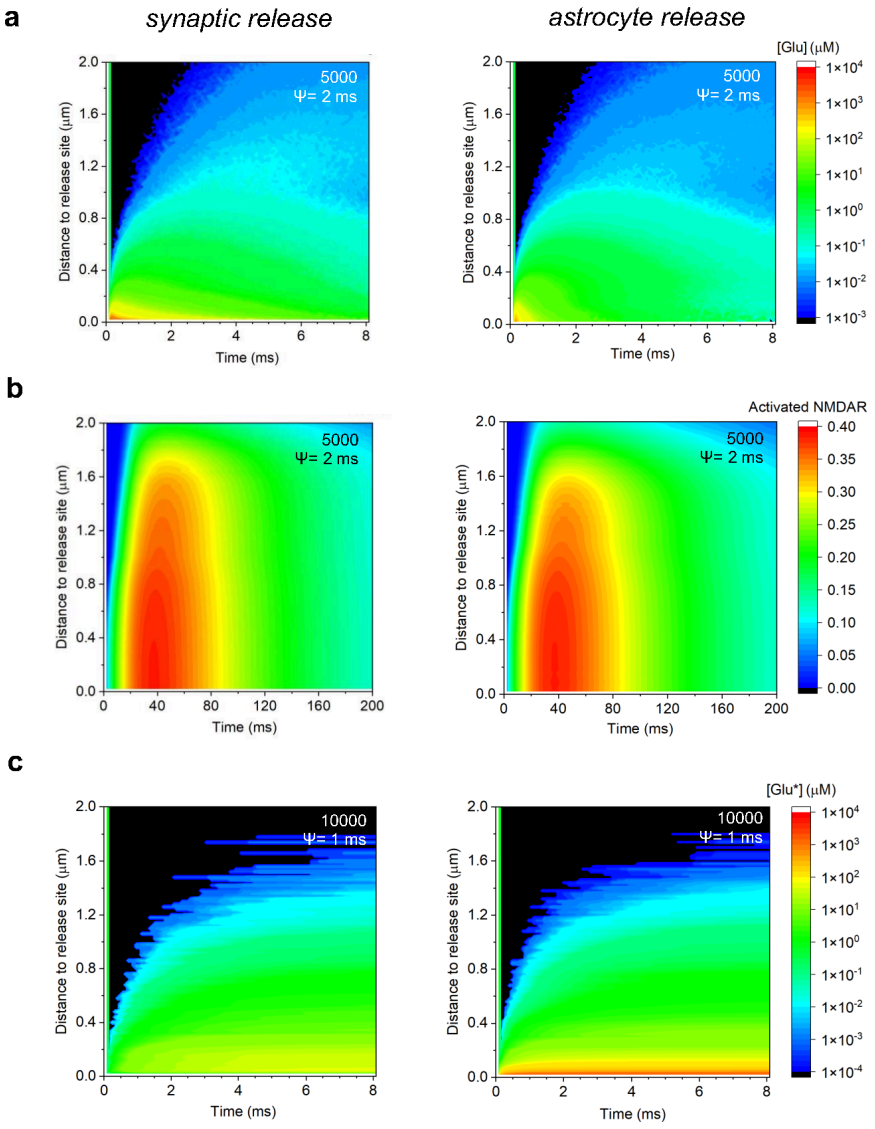

Figure 4

Comparing escape actions of glutamate released from synapses and from astrocytes.

(a) The spatiotemporal dynamics of the free glutamate concentration in a simulation experiment in which 5000 glutamate molecules were released either at the synaptic cleft (*left*) or from the astrocyte

surface (*right*). General neuropil parameters are as in Fig. 1a; glutamate transporters are distributed on astroglial element surfaces only (volume fraction ~10%), at a density which corresponds to Ψ = 2 ms.

(b) The spatiotemporal dynamics of NMDA receptor activation, assuming no Mg^{2+} block, computed based on the free glutamate dynamics as shown in the corresponding panels in **a**; see Methods for further detail.

(c) Example of the spatiotemporal dynamics of the bound-glutamate concentration ([Glu*]) in a simulation experiment in which 10000 glutamate molecules were released either at the synaptic cleft (*left*) or from the astrocyte surface (*right*). General neuropil parameters are as in Fig. 1a; glutamate transporters are distributed on astroglial element surfaces only (volume fraction ~10%), at a density which corresponds to Ψ = 2 ms. Note a high concentration of bound glutamate near the astrocytic release site (*right*).

Supplementary Files

This is a list of supplementary files associated with this preprint. Click to download.

- SupplementaryFigs.pdf